Selective Binding of Carotenoids with a Shorter Conjugated Chain to the LH2 Antenna Complex and Those with a Longer Conjugated Chain to the Reaction Center from *Rubrivivax gelatinosus*†

Yoshinori Kakitani,‡ Ritsuko Fujii,‡,§ Yoshihiro Hayakawa,‡ Masahiro Kurahashi,‡ Yasushi Koyama,*,‡ Jiro Harada,||,⊥ and Keizo Shimada||

Faculty of Science and Technology, Kwansei Gakuin University, 2-1 Gakuen, Sanda 669-1337, Japan, and Department of Biological Sciences, Tokyo Metropolitan University, 1-1 Minami-Ohsawa, Hachioji 192-0397, Japan

Received December 3, 2006; Revised Manuscript Received April 14, 2007

ABSTRACT: *Rubrivivax gelatinosus* having both the spheroidene and spirilloxanthin biosynthetic pathways produces carotenoids (Cars) with a variety of conjugated chains, which consist of different numbers of conjugated double bonds (*n*), including the C═C (*m*) and C═O (*o*) bonds. When grown under anaerobic conditions, the wild type produces Cars for which $n = m = 9-13$, whereas under semiaerobic conditions, it additionally produces Cars for which $n = m + o = 10 + 1$, $13 + 1$, and $13 + 2$. On the other hand, a mutant, in which the latter pathway is genetically blocked, produces only Cars for which $n = 9$ and 10 under anaerobic conditions and $n = 9$, 10, and $10 + 1$ under semianaerobic conditions. Those Cars that were extracted from the LH2 complex (LH2) and the reaction center (RC), isolated from the wild-type and the mutant *Rvi. gelatinosus*, were analyzed by HPLC, and their structures were determined by mass spectrometry and ^{1}H NMR spectroscopy. The selective binding of Cars to those pigment−protein complexes has been characterized as follows. (1) Cars with a shorter conjugated chain are selectively bound to LH2 whereas Cars with a longer conjugated chain to the RC. (2) Shorter chain Cars with a hydroxyl group are bound to LH2 almost exclusively. This rule holds either in the absence or in the presence of the keto group. The natural selection of shorter chain Cars by LH2 and longer chain Cars by the RC is discussed, on the basis of the results now available, in relation to the light-harvesting and photoprotective functions of Cars.

Carotenoids (Cars)[1] in bacterial photosynthesis have dual functions of light harvesting and photoprotection (*1*). In the former function, Cars harvest light energy in the blue-green region where bacteriochlorophylls (BChls) do not, whereas in the latter function, Cars protect the photosynthetic system against degradation by harmful singlet oxygen that is generated by triplet-energy transfer from BChls. More specifically, the light-harvesting function includes the absorption of light by Car followed by singlet-energy transfer to BChl, whereas the photoprotective function includes triplet-energy transfer from BChl to Car followed by the dissipation of the triplet energy by Car. Presumably, the major function of Cars in the LH1 and LH2 antenna complexes (hereafter, abbreviated as LH1 and LH2, respectively, or collectively as LHC) is light harvesting, while that of Cars in the reaction center (RC) is photoprotection, although Cars bound to the RC play the light-harvesting function and Cars bound to LHC play the photoprotective function, as well.

Most recently, it has been found that photosynthetic light harvesting, in excess light, is regulated by a process as feedback deactivation by the use of the radical cation of a Car, zeaxanthin (*2*). Further, intermolecular Car-to-(B)Chl radical cation electron-transfer reactions have been identified in the photosystem II reaction center (*3*) and in bacterial LH1 antenna complexes (*4*). There can be "a redox photoprotective function of Cars".

† This work has been supported by an "Open Research Center Project" grant (Y. Koyama), Grant-in-Aid 15770100 (R.F.) from the Ministry of Education, Culture, Sports, Science and Technology, Japan, and an international joint research grant from NEDO (New Energy and Industrial Technology Development Organization). Y. Kakitani has been supported by Research Fellowships of the Japan Society for the Promotion of Science for Young Scientists.

* To whom correspondence should be addressed. Telephone and fax: +81-79-565-8408. E-mail: ykoyama@kwansei.ac.jp.

‡ Kwansei Gakuin University.

§ Current address: Department of Physics, Graduate School of Science, Osaka City University, Sugimoto, Sumiyoshi-ku, Osaka 558-8585, Japan.

|| Tokyo Metropolitan University.

⊥ Current address: Department of Bioscience and Biotechnology, Ritsumeikan University, Kusatsu 525-8577, Japan.

[1] Abbreviations: ADC(2)-x, extended second-order algebraic diagrammatic construction; ampicillin, D-(−)-α-aminobenzylpenicillin; BChl, bacteriochlorophyll; Car, carotenoid; COSY, correlation spectroscopy; DEPT, distortionless enhancement by polarization transfer; hfs, high-field shift(s); HPLC, high-pressure liquid chromatography; LDAO, *N*,*N*-dimethyldodecylamine-*N*-oxide; lfs, low-field shift(s); LH1, light-harvesting complex 1; LH2, light-harvesting complex 2; LHC, light-harvesting complexes; lhs, left-hand side; *m*, number of conjugated C═C bonds; *n*, number of conjugated double bonds ($m + o$); NMR, nuclear magnetic resonance; *o*, number of conjugated C═O bonds; OD, optical density; P, special-pair bacteriochlorophylls; PPP-MRD-CI, Pariser−Parr−Pople multireference double-excitation configurational interactions; RC, reaction center; rhs, right-hand side; ROESY, rotating-frame Overhauser enhancement spectroscopy; S_0, ground state; T_1, lowest triplet state.

10.1021/bi602485x CCC: $37.00
Published on Web 05/26/2007

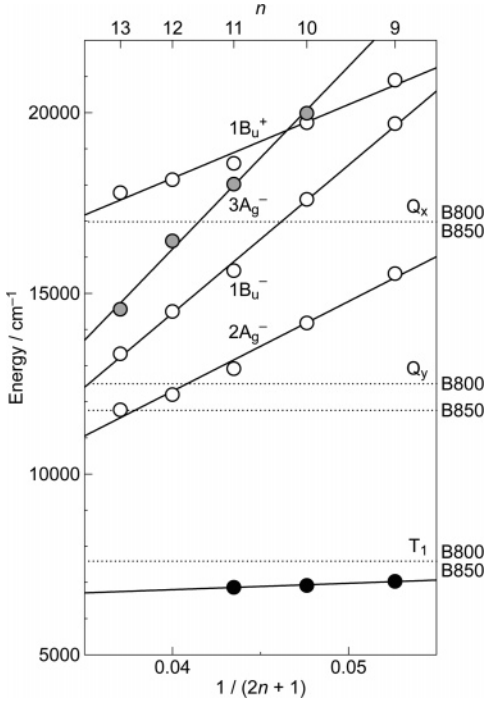

FIGURE 1: Dependence of the singlet-state ($1B_u^+$, $3A_g^-$, $1B_u^-$, and $2A_g^-$) and triplet-state (T_1) energies on the number of conjugated double bonds (n) of Cars. The $1B_u^+$, $3A_g^-$, $1B_u^-$, and $2A_g^-$ energies were determined by measurement of resonance Raman excitation profiles of mini-9-β-carotene ($n = 9$), spheroidene ($n = 10$), lycopene ($n = 11$), anhydrorhodovibrin ($n = 12$), and spirilloxanthin ($n = 13$) in the solid state (*7*−*9*). The T_1 energies were determined by high-sensitivity emission spectroscopy of neurosporene ($n = 9$), spheroidene ($n = 10$), and lycopene and rhodopin (both $n = 11$) bound to LH2 from *Rba. sphaeroides* G1C, *Rba. sphaeroides* 2.4.1, and *Rsp. molischianum* (*55*). The singlet-state (Q_x and Q_y) and triplet-state (T_1) energies of BChl *a* bound to LH2 are also shown for comparison; the former were determined by conventional absorption spectroscopy and the latter by high-sensitivity emission spectroscopy (*55*).

A natural selection of the Car configurations, i.e., the all-*trans* configuration by LHC versus the 15-*cis* configuration by the RC, has been found (*5*, *6*). The reason for the selection of the all-*trans* configuration by LHC has been explained as follows. Figure 1 (the top part) shows an energy diagram for the low-lying singlet states of Cars as functions of $1/(2n + 1)$, where n is the number of conjugated double bonds. The approximate C_{2h} symmetry of the stretched conjugated chain gives rise to low-lying singlet states having different symmetries, including $1B_u^+$, $3A_g^-$, $1B_u^-$, and $2A_g^-$; the $1B_u^-$ and $3A_g^-$ states were found recently (*7*−*9*). According to the selection rule (*10*, *11*), the ionic $1B_u^+$ state can be populated by absorptive transition from the ground $1A_g^-$ state, whereas the covalent $3A_g^-$, $1B_u^-$, and $2A_g^-$ states can be populated only by internal conversion from the $1B_u^+$ state (*12*). It has been shown that the Car-to-BChl singlet-energy transfer takes place through plural channels, i.e., starting from the $1B_u^+$, $1B_u^-$, and $2A_g^-$ states, during the internal-conversion processes in LH1 and LH2 (*13*−*15*), explaining the reason for the selection of the all-*trans* configuration. The role of the $3A_g^-$ state (shown with gray circles in Figure 1) remains to be elucidated.

The notation of the singlet states of Cars used in this report is based on the extrapolation of the results of theoretical calculations. The ordering of the state energies and the slopes of state energies as linear functions of $1/(2n + 1)$ in an ≈2:3:4 $2A_g^-$:$1B_u^-$:$3A_g^-$ ratio, which were determined by resonance Raman (*9*), electronic absorption (*16*), and fluorescence (summarized in ref *9*) spectroscopies, were in good agreement with those obtained by the PPP-MRD-CI (Pariser−Parr−Pople multireference double-excitation configurational interactions) calculations (*17*). Most recently, the ADC(2)-x (extended second-order algebraic diagrammatic construction) calculations reproduced the state ordering of $1B_u^+ > 1B_u^- > 2A_g^-$ and the slopes of linear functions in a 2:2.4 $2A_g^-$:$1B_u^-$ ratio (*18*). The symmetry of each singlet state has not been determined experimentally yet. Other proposals of singlet states, including the S* state (*19*), the S_x state (*20*), the $S^‡$ state (*21*), and the vibrationally hot $2A_g^-$ state (*22*), have also been made. Therefore, the singlet-state energies of Cars are still a matter of debate.

The selection of the 15-*cis* configuration by the RC has been ascribed to its potential for rapid isomerization toward the all-*trans* configuration upon triplet excitation (*23*−*26*). The rotational motion around the C═C bonds, even in the binding pocket of the RC, can cause a change in the orbital angular momentum and, as a result, a change in the spin angular momentum through the spin−orbit coupling. This enhances the T_1 (triplet) → S_0 (ground) intersystem crossing, accompanying the dissipation of triplet energy (*27*−*29*).

Figure 1 (the bottom part) also depicts the triplet energies of BChl and Car in LH2. Since the light-harvesting function includes the Car-to-BChl singlet-energy transfer, whereas the photoprotective function includes the BChl-to-Car triplet-energy transfer, and since the singlet- and triplet-state energies are reduced with n as linear functions of $1/(2n + 1)$, it is naturally expected that those Cars having a smaller n (as a result, a higher singlet energy) are advantageous for the light-harvesting function whereas those having a larger n (a lower triplet energy) for the photoprotective function. However, this idea needs to be proven in the real photosynthetic system.

In a previous investigation, we examined a set of Cars ($n = 11$−13) that were produced through the spirilloxanthin pathway in *Rhodobium marinum* (*30*); we found the preferential binding of the precursors ($n = 11$ and 12) to LH1 and that of spirilloxanthin ($n = 13$) to the RC. This preferential binding supports the idea described above of the natural selection of the Car conjugation lengths by LHC and the RC for the light-harvesting and photoprotective functions, respectively.

Figure 2 shows the spheroidene pathway on the left-hand side (hereafter abbreviated as lhs) and the spirilloxanthin pathway on the right-hand side (rhs) in *Rubrivivax gelatinosus*. In the wild type, both pathways function (*31*), but in the mutant, the spirilloxanthin pathway is genetically blocked (*32*). Hereafter, we will call the numbers of conjugated C═C and C═O bonds m and o, respectively, and their sum (the number of conjugated double bonds) $n = m + o$. When grown under anaerobic conditions, wild-type *Rvi. gelatinosus* produces a variety of Cars for which $n = m = 9$−13. When grown under semiaerobic conditions, it produces keto-Cars to further increase the conjugation length (n) to $10 + 1$ in the spheroidene pathway and to $13 + 1$ and $13 + 2$ in the spirilloxanthin pathway. A mutant, the spirilloxanthin pathway of which had been genetically blocked, was also used to artificially reduce the number of conjugated chains

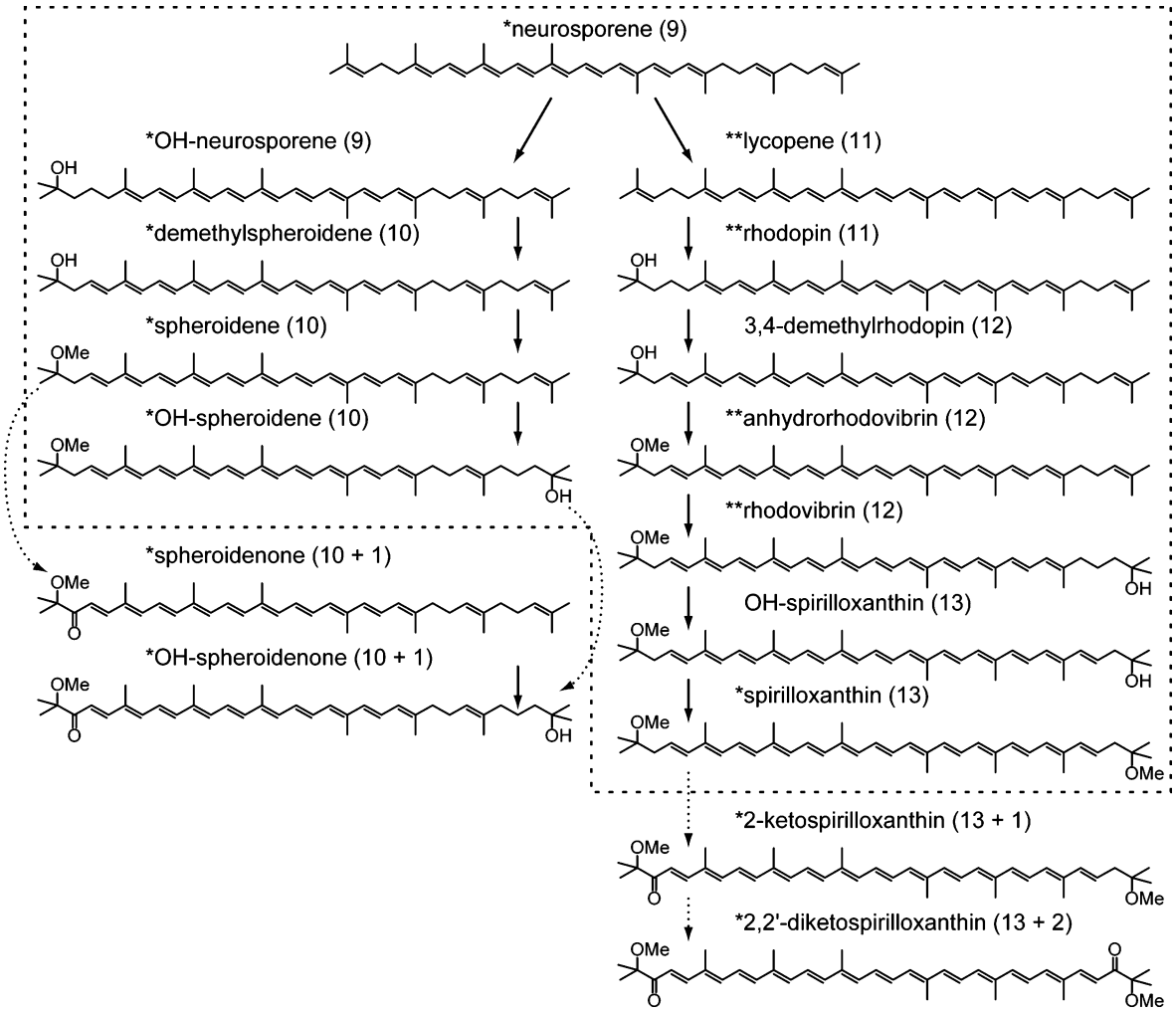

FIGURE 2: Car biosynthetic pathways in *Rvi. gelatinosus*, which include the spheroidene pathway (lhs) and the spirilloxanthin (rhs) pathway. Those Cars surrounded by a dashed line are synthesized when the wild-type cells are grown under anaerobic conditions. Keto derivatives outside of the dashed line can be produced (dotted arrows on both sides) when the cells are grown under semiaerobic conditions. In the mutant (ΔI-I_{Rc}), the spirilloxanthin pathway is genetically blocked.

available under anaerobic and semiaerobic conditions (n = 9, 10, and 10 + 1). Combination of the wild-type and mutant strains grown under both culturing conditions has provided us with four different sets of Cars so we can examine whether such selective binding is present between LH2 and the RC.

Thus, we have addressed the question of whether natural selection of the conjugation length between LH2 and the RC has been developed in *Rvi. gelatinosus* that produces a variety of Cars. Actually, we have obtained a positive answer to this question and discussed the mechanisms and the reasons for the selective binding based on the data now available concerning the Car binding sites and the excited-state dynamics of Cars.

MATERIALS AND METHODS

Culturing the Cells of Rvi. gelatinosus and Preparation of LH2 and the RC. Wild-type *Rvi. gelatinosus* (strain IL144) and a genetically engineered mutant (ΔI-I_{Rc}) were grown in PYS medium [0.5% polypeptone, 0.1% yeast extract, 0.5% sodium succinate, and minerals (pH 7.0)] (*33*) without and with ampicillin (50 μg/mL), respectively (*32*). This mutant was constructed by deleting the *crtI* gene which encodes the phytoene desaturase synthesizing both neurosporene and lycopene and by introducing the *crtI* gene from *Rhodobacter sphaeroides* synthesizing neurosporene. The cells were grown under anaerobic conditions at 29−30 °C in the light (3000−4000 Lux) for 17−23 h after incubation in the dark for 5−8 h. In the semiaerobic culturing, the cell suspension was bubbled with air in the last 5 h of culturing in the light. To change the Car composition bound to well-developed photosynthetic pigment−protein complexes, we used this culturing condition (we call this the "semiaerobic" condition), which probably corresponds to "insufficient aeration" described in ref *34*.

Chromatophores (12000−200000*g* fraction) were obtained by disruption of the cells using a French press (1450 kg/cm^2) followed by centrifugation. For the preparation of LH2, the chromatophores (OD_{Q_y} = 50 cm^{-1}) were suspended in a buffer [20 mM Tris-HCl (pH 8.0) (hereafter, called "Tris buffer")] and solubilized with 1.5% *N*,*N*-dimethyldodecylamine-*N*-oxide (LDAO; Fluka Chemie GmbH) at 0 °C for 45 min. The suspension was diluted into twice the volume with Tris buffer and applied to a DE52 column (Whatman International Ltd.) after centrifugation (25000*g* and 4 °C for 10 min). The LH2 component eluted at 100 mM NaCl in Tris buffer containing 0.1% LDAO; NaCl in the buffer was removed by dialysis. For the preparation of the RC, the chromatophores (OD_{Q_y} = 50 cm^{-1}) were solubilized at 0 °C

for 30 min in Tris buffer containing 1.0% LDAO. The resultant suspension was applied to a DE52 column after centrifugation (200000*g* and 4 °C for 60 min). The RC component eluted at 50 mM NaCl in Tris buffer containing 0.05% LDAO; again, NaCl was removed by dialysis.

HPLC Analysis of the Car Extracts from LH2 and the RC. Cars were extracted from LH2 and the RC as follows. The suspension of LH2 or the RC in Tris buffer with 0.1 or 0.05% LDAO (OD × $V = \sim 5$ cm^{-1} mL) was loaded onto a DE52 column, washed with 1 column volume of distilled water, and then dried with a stream of nitrogen gas. All the pigments were extracted from the column by addition of ~10 mL of a mixture of methanol and acetone (2:7). The extract was dried up with nitrogen gas and then dissolved into the eluent for high-pressure liquid chromatography (HPLC) analyses. The HPLC analysis of the extracted Cars was performed under the following conditions: column, a home-packed silica-gel, Lichrosorb Si-60 (5 μs; Merck GmbH) column [4.6 mm (inside diameter) × 300 mm]; eluent, 1.5% acetone in benzene (v/v); flow rate, 0.8 mL/min; and detection wavelengths, 350−800 nm by using a photodiode array detector (Waters 996; Waters Corp.).

Mass Spectrometry and ^{1}H NMR Spectroscopy. Electron-impact ionization mass spectra were recorded in chloroform as reported previously (*30*). A set of 600 MHz ^{1}H nuclear magnetic resonance (NMR) spectra, including ^{1}H−^{1}H COSY (correlation spectroscopy) and ^{1}H−^{1}H ROESY (rotating-frame Overhauser enhancement spectroscopy) spectra, were recorded for spirilloxanthin, 2-ketospirilloxanthin, and 2,2′-diketospirilloxanthin, having the longest conjugated chains, on a Bruker Avance 600 DRX spectrometer equipped with a Bruker/SGI workstation. A set of 400 MHz ^{1}H NMR spectra were recorded for the rest of the Cars as reported previously (*30*). In both measurements, tetramethylsilane was used as an internal standard. A set of one-dimensional spectra (digital resolution, 0.18 and 0.24 Hz, respectively) and the two-dimensional spectra (digital resolution, 5.87 and 6.83 Hz, respectively) mentioned above was used to assign the ^{1}H signals of each extracted Car.

RESULTS

Identification of Carotenoids in LH2 and the RC

Figure 3 exhibits the HPLC elution profiles for the Car extracts from LH2 and the RC of the wild type grown under anaerobic and semiaerobic conditions (the top left and right panels) and those of the mutant grown under anaerobic and semiaerobic conditions (the bottom left and right panels). The assignment of each peak, which was obtained by the structural determination to be described below, is indicated. Ten different kinds of Cars, in total, were identified by silica gel chromatography; those Cars are indicated by single asterisks in Figure 2. A set of four different Cars in the spirilloxanthin pathway, which had been identified by silica gel chromatography in a previous investigation of *Rbi. marinum* (indicated by double asterisks) (*30*), were not identified in this present investigation, suggesting that the harvested cells were in a stationary phase as far as the pair of biosynthetic pathways was concerned.

Figure 4 depicts the chemical structures of the 10 Cars, which can be characterized in terms of the combination of one half of each Car structure (hereafter, called "half-structures"). Neurosporene, chloroxanthin (which we call OH-neurosporene), demethylspheroidene, and spheroidene have four different half-structures on the lhs (a−d, respectively) and share half-structure (a′) on the rhs. OH-Spheroidene also has a half-structure (d) on the lhs and another half-structure (b′) on the rhs. Spheroidenone and OH-spheroidenone share a fifth half-structure (e) on the lhs and have the above-mentioned half-structures on the rhs (a′ and b′, respectively). Spirilloxanthin and 2,2′-diketospirilloxanthin consist of a pair of half-structures (d and e, respectively); 2-ketospirilloxanthin between them consists of one each. The assignment of each Car has been made by means of mass spectrometry and ^{1}H NMR spectroscopy, taking advantage of the structural characterization described above.

Table 1 lists mass spectrometry data for the seven Cars except for the standard set of Cars, i.e., neurosporene, spheroidene, and spirilloxanthin, whose correlations between the structures and the mass spectroscopy data have been well-documented (*35*). The excellent agreement, within the limit of experimental error (±0.0017 atomic mass unit), between the observed and calculated *m*/*z* values of the molecular ion peak proves the assignment of each Car in the table. Main fragment peaks are also assigned by the use of each molecular weight (M). The M − 18 peaks indicating the removal of a water molecule, appearing in OH-neurosporene, demethylspheroidene, and OH-spheroidenone, confirm the half-structures (b, c, and b′), respectively. The fragment peak of 69 appearing in OH-neurosporene and demethylspheroidene confirms the half-structure (a′), and the fragment peak of 73 appearing in the rest of the Cars confirms the half-structures (d and e). The ratios of the two fragment peaks produced by in-chain reactions, i.e., M − 92 (toluene) and M − 106 (xylene), nicely reflect the numbers of C═C bonds, 9 (0.89), 10 (0.12−0.17), and 13 (0.015−0.016) (*35*). The presence or absence of the C═O bond(s) does not affect the value at all (*35*). Thus, mass spectrometry has precisely determined the molecular weight and partially characterized the molecular structure of each Car.

Table 2 lists the values of the ^{1}H chemical shifts for the 10 Cars. The structure of each Car can be characterized as follows, starting from the set of standard Cars, i.e., neurosporene, spheroidene, and spirilloxanthin, whose correlations between the structures and the ^{1}H chemical shifts have been well-established by the use of NMR spectroscopies (*36*−*39*),[2] including ^{1}H−^{1}H COSY, ^{1}H−^{1}H ROESY, ^{13}C DEPT (distortionless enhancement by polarization transfer), and ^{13}C−^{1}H COSY (see both Table 2 and Figure 4). (i) With the transition from neurosporene to OH-neurosporene (a, a′ → b, a′), the high-field shifts (hfs) of the methyl and olefinic ^{1}H signals take place due to the electron donated by the OH group (see the underlined values in the table), the rest of the values being unchanged. (ii) With the transition from spheroidene to demethylspheroidene (d, a′ → c, a′), the methoxy ^{1}H signal disappears and the 1Me-^{1}H signal shifts to the lower field, the other chemical shifts being unchanged. (iii) With the transition from spheroidene to OH-spheroidene (d, a′ → d, b′), the hfs of the methyl and olefinic ^{1}H signals

[2] The chemical shifts of ^{1}H signals we obtained in this investigation were in agreement with those in the literature within the limit of experimental error (0.01 ppm).

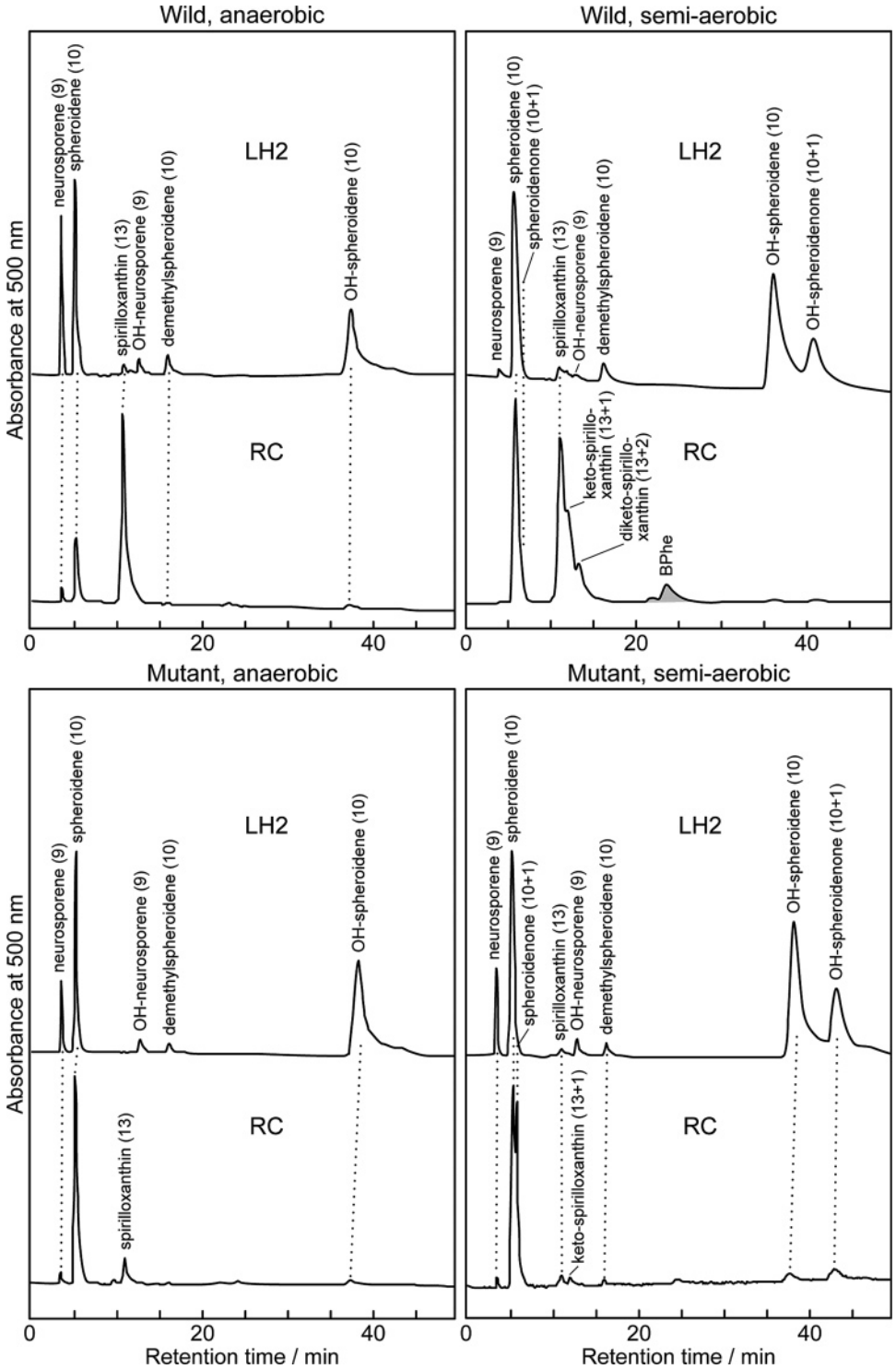

FIGURE 3: HPLC elution profiles of the Car extracts from LH2 and the RC of the wild type (top) and the mutant (bottom) grown under anaerobic (lhs) and semiaerobic (rhs) conditions. The chemical structures of those Cars are shown in Figure 4.

take place in the vicinity of the OH group newly introduced as in case (i). (iv) With the transition from spheroidene to spheroidenone (d, a′ → e, a′), large low-field shifts (lfs) of the methyl and olefinic ^{1}H signals take place not only in the vicinity of the C═O group but also in the extended part of the conjugated chain, most probably due to the strong electron-withdrawing effect of the keto group that is introduced. (v) With the further transition to OH-spheroidenone (e, a′ → e, b′), the hfs of the methyl and the olefinic ^{1}H signals additionally take place as in both cases of introducing the hydroxyl group in spheroidene (d, a′ → d, b′) and spheroidenone (e, a′ → e, b′). (vi) With the transition from spirilloxanthin to keto- or diketospirilloxanthin (d, d → e, d or d, d → e, e, respectively), the introduction of one or two keto C═O groups causes the large lfs of the relevant methyl and olefinic ^{1}H signals in an extended region, as in case (iv) on going from spheroidene to spheroidenone (d, a′ → e, a′). The values of the ^{1}H chemical shifts of the standard neurosporene, spheroidene, and spirilloxanthin can be easily

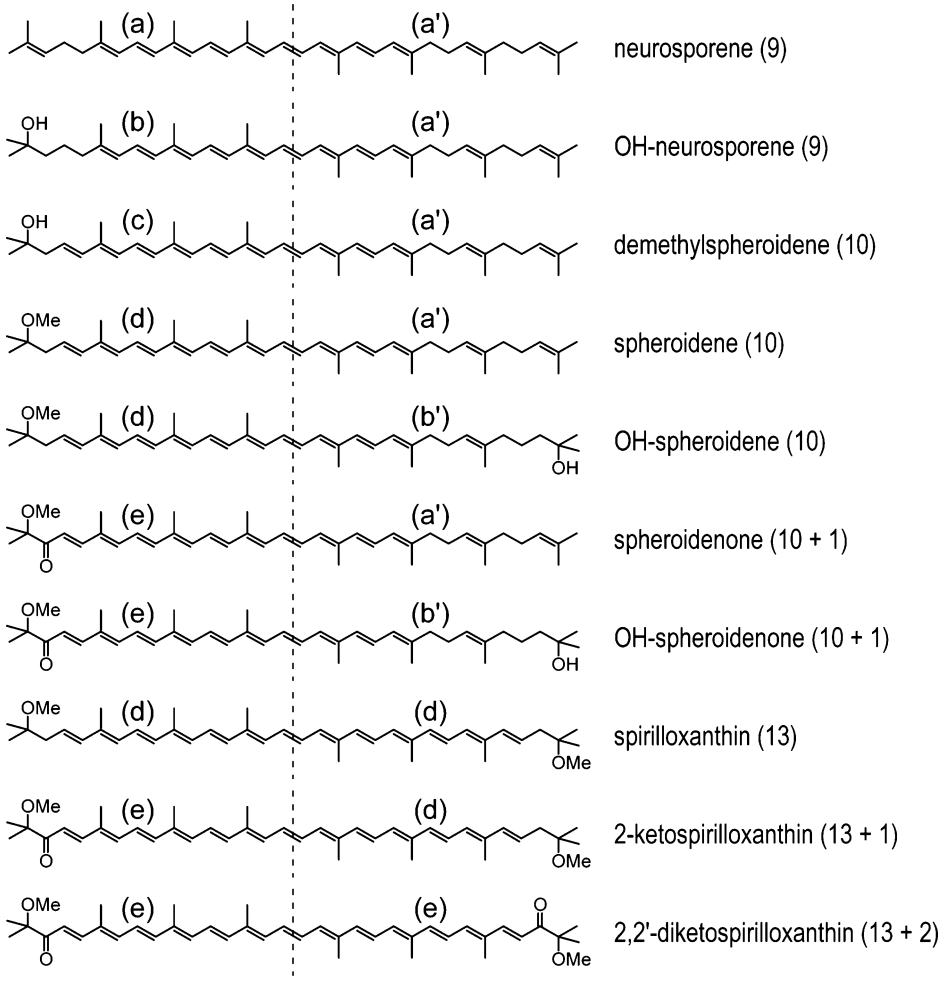

FIGURE 4: Chemical structures of Cars identified in this investigation. The numbers of C=C and C=O bonds are indicated as Car ($m + o$). All the Car structures can be characterized in terms of half-structures a−e appearing on the lhs and a′ and b′ appearing specifically on the rhs of the vertical dashed line.

Table 1: Mass Spectrometry Data for Carotenoids Isolated from LH2 and the RC of *Rvi. gelatinosus*

carotenoids (n)	atomic composition	molecular ion peak		main fragments	(M − 92)/(M − 106)
		observed	calculated		
OH-neurosporene (9)	$C_{40}H_{60}O$	556.4632	556.4641	450 (M − 106), 464 (M − 92), 538 (M − 18), 69, 81	0.89
demethylspheroidene (10)	$C_{40}H_{58}O$	554.4471	554.4484	448 (M − 106), 462 (M − 92), 536 (M − 18), 69	0.17
OH-spheroidene (10)	$C_{41}H_{62}O_2$	586.4749	586.4746	480 (M − 106), 494 (M − 92), 73	0.12
spheroidenone (10 + 1)	$C_{41}H_{58}O_2$	582.4425	582.4433	476 (M − 106), 490 (M − 92), 73	0.16
OH-spheroidenone (10 + 1)	$C_{41}H_{60}O_3$	600.4523	600.4540	476 (M − 124), 494 (M − 106), 508 (M − 92), 582 (M − 18), 73	0.17
2-ketospirilloxanthin (13 + 1)	$C_{42}H_{58}O_3$	610.4385	610.4383	472 (M − 138), 504 (M − 106), 518 (M − 92), 578 (M − 32), 73	0.015
2,2′-diketospirilloxanthin (13 + 2)	$C_{42}H_{56}O_4$	624.4174	624.4175	518 (M − 106), 532 (M − 92), 73	0.016

confirmed in terms of the ^{1}H chemical shifts of half-structures a, a′, and d.

As shown above, each unique set of chemical shift values can be nicely explained in terms of the combination of half-structures, within the limit of experimental error (±0.03 ppm). The fact proves that both the chemical structures of Cars and the assignment of the ^{1}H signals are correct.

Selective Binding of Cars to LH2 and the RC

Figure 5 depicts the compositions of Cars extracted from LH2 (top panels) and the RC (bottom panels) that were isolated from the wild type (the lhs panels) and the mutant (the rhs panels) grown under anaerobic (left) and semiaerobic (right) conditions. Here, the abscissa scale is indicated by m, and each Car is specified as Car (m) or Car ($m + o$). The values of Car compositions (in mole percent) are listed for chromatophores, LH2, and the RC in Table S1 of the Supporting Information.

Wild Type, Grown under Anaerobic Conditions. Shorter chain Car ($n = 9$) and Car ($n = 10$) are preferentially bound to LH2, whereas the longest chain Car ($n = 13$) is bound to the RC almost exclusively. Shorter chain OH-Cars are exclusively bound to LH2.

Table 2: ^{1}H Chemical Shift Values (δ in parts per million) for Isolated Carotenoids from LH2 and the RC of *Rvi. gelatinosus* (in chloroform-*d* solution)

proton	neuro-sporene	OH-neuro-sporene	demethyl-spheroidene	spher-oidene	OH-spher-oidene	spheroi-denone	OH-spheroi-denone	spirillo-xanthin	2-ketospirillo-xanthin	2,2′-diketospirillo-xanthin
	a	b	c	d	d	e	e	d	e	e
1OH	–	nd	nd	–	–	–	–	–	–	–
1OMe	–	–	–	3.23	3.23	3.22	3.22	3.24	3.22	3.22
1Me^1	1.66	1.20	1.24	1.16	1.16	1.35	1.35	1.16	1.36	1.36
1Me^2	1.58	1.20	1.24	1.16	1.16	1.35	1.35	1.16	1.36	1.36
2H	5.09	1.42	2.31	2.32	2.32	–	–	2.33	–	–
3H	2.11	2.00	5.75	5.72	5.72	6.76	6.76	5.72	6.77	6.78
4H	2.06	2.13	6.21	6.16	6.16	7.47	7.47	6.17	7.48	7.48
5Me	1.80	1.82	1.93	1.93	1.93	1.99	1.99	1.93	2.00	2.00
6H	5.94	5.95	6.13	6.11	6.11	6.61	6.61	6.12	6.62	6.63
7H	6.47	6.50	6.59	6.59	6.60	6.56	6.56	6.61	6.63	6.64
8H	6.23	6.24	6.36	6.34	6.35	6.58	6.58	6.36	6.56	6.56
9Me	1.95	1.95	1.98	1.98	1.98	2.00	2.00	1.98	1.99	2.00
10H	6.16	6.18	6.21	6.25	6.23	6.34	6.34	6.24	6.36	6.36
11H	6.61	6.62	6.63	6.62	6.63	6.63	6.63	6.65	6.65	6.66
12H	6.33	6.35	6.38	6.38	6.37	6.45	6.44	6.39	6.46	6.46
13Me	1.95	1.96	1.96	1.96	1.97	1.97	1.97	1.99	2.01	2.01
14H	6.21	6.24	6.26	6.22	6.26	6.31	6.31	6.28	6.33	6.34
15H	6.59	6.59	6.61	6.61	6.62	6.61	6.61	6.65	6.66	6.69
15′H	6.61	6.63	6.64	6.61	6.63	6.67	6.67	6.65	6.70	6.69
14″	6.18	6.20	6.21	6.20	6.20	6.21	6.21	6.28	6.29	6.34
13′Me	1.93	1.96	1.95	1.95	1.95	1.96	1.96	1.99	2.00	2.01
12′H	6.22	6.25	6.24	6.24	6.24	6.24	6.24	6.39	6.40	6.46
11′H	6.48	6.49	6.50	6.50	6.50	6.52	6.52	6.65	6.67	6.66
10′H	5.94	5.95	5.96	5.96	5.95	5.96	5.96	6.24	6.24	6.36
9′Me	1.80	1.82	1.82	1.82	1.82	1.83	1.83	1.98	1.99	2.00
8′H	2.10	2.13	2.13	2.12	2.13	2.13	2.13	6.36	6.37	6.56
7′H	2.11	2.13	2.13	2.12	2.13	2.13	2.13	6.61	6.61	6.64
6′H	5.09	5.12	5.12	5.12	5.12	5.12	5.12	6.12	6.12	6.63
5′Me	1.59	1.60	1.61	1.61	1.60	1.60	1.60	1.93	1.94	2.00
4′H	1.96	2.00	1.98	2.00	1.98	1.97	1.98	6.17	6.17	7.48
3′H	2.04	2.00	2.06	2.05	1.51	2.06	1.51	5.72	5.72	6.78
2′H	5.07	5.11	5.08	5.08	1.42	5.09	1.42	2.33	2.33	–
1′Me^1	1.59	1.61	1.60	1.60	1.20	1.62	1.20	1.16	1.16	1.36
1′Me^2	1.67	1.69	1.68	1.68	1.20	1.68	1.20	1.16	1.16	1.36
1′OMe	–	–	–	–	–	–	–	3.24	3.24	3.22
1′OH	–	–	–	–	nd	–	nd	–	–	–
	a′	a′	a′	a′	b′	a′	b′	d	d	e

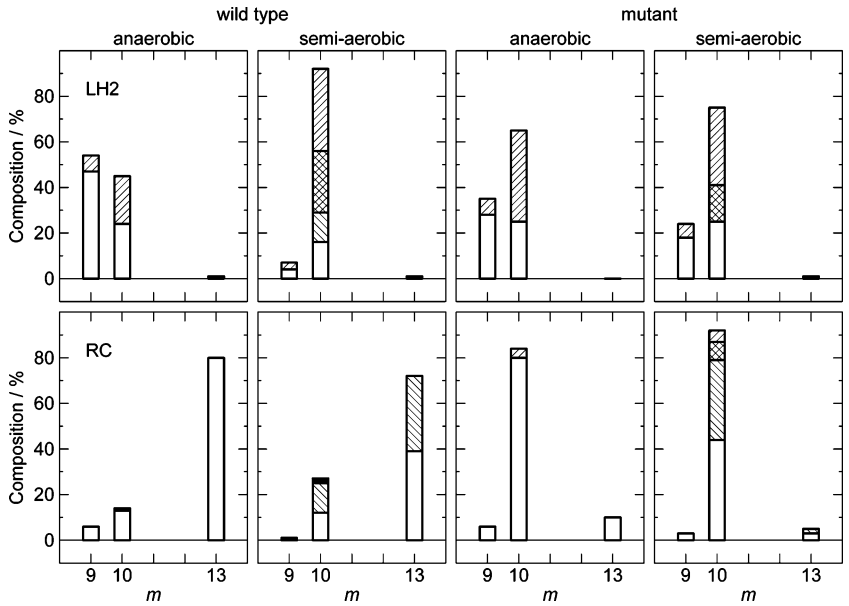

FIGURE 5: Selection of the Car-conjugated chains by LH2 (top) and the RC (bottom) in the wild type (lhs) and the mutant (rhs), grown under anaerobic (left) and semiaerobic (right) conditions. Cars are classified by the number of conjugated C=C bonds (*m*). The conjugated chains of those Cars are classified into OH-Cars (top right to bottom left, oblique lines), keto-Cars (top left to bottom right, oblique lines), keto-Cars with the OH group (crossed oblique lines), and Cars with neither the OH nor the keto group (white bars).

Wild Type, Grown under Semiaerobic Conditions. Car ($n = 10$) and keto-Car ($n = 10 + 1$) with the OH group are exclusively bound to LH2, and Car ($n = 10$) and keto-Car ($n = 10 + 1$) without the OH group also are preferentially

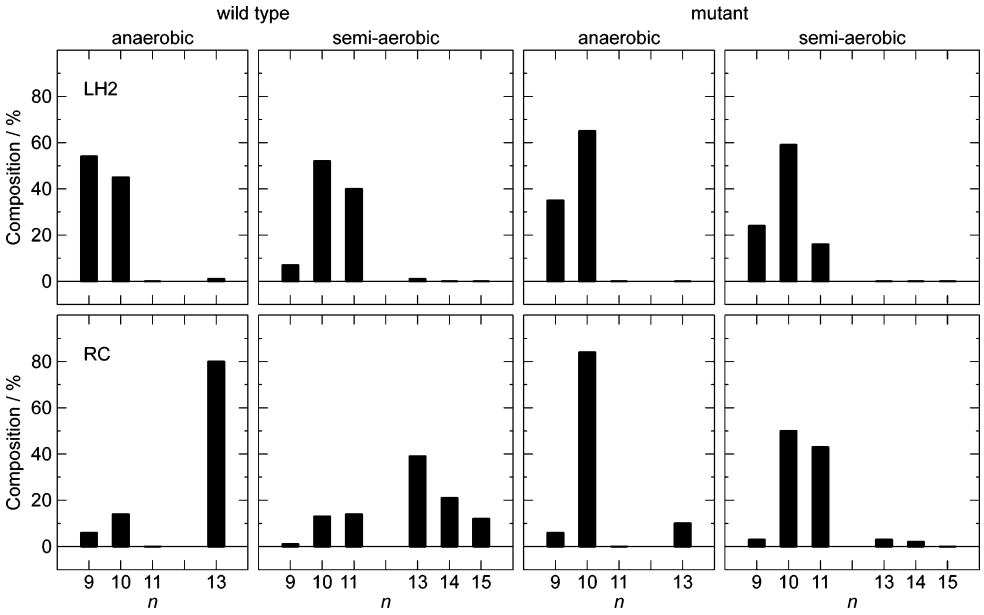

FIGURE 6: Selection of the Car conjugation lengths by LH2 (top) and the RC (bottom) from the wild type (lhs) and the mutant (rhs), grown under anaerobic (left) and semiaerobic (right) conditions. Cars are classified by the number of conjugated double bonds ($n = m + o$), including the C═C (m) and C═O (o) bonds; no differentiation is made between the presence or absence of the OH group.

bound to LH2. On the other hand, Car ($n = 13$) and its mono- and diketo derivatives, i.e., Car ($n = 13 + 1$) and Car ($n = 13 + 2$), respectively, are exclusively bound to the RC.

Mutant, Grown under Anaerobic Conditions. Car ($n = 9$) and Car ($n = 10$) with and without the OH group are bound to LH2, whereas Car ($n = 10$), the longest chain Car that is readily available, is preferentially bound to the RC. It is interesting that even OH-Car ($n = 10$) and Car ($n = 13$) are bound to the RC. The following observations strongly suggest the selective binding of the longest chain Car, i.e., spirilloxanthin, to the RC. When the *crtI* gene of *Rba. sphaeroides* that was introduced into this mutant was overexpressed in *Escherichia coli* with a phytoene synthesis background, a small amount of lycopene, the precursor of spirilloxanthin, was detected (showing a leakage) with a significant amount of neurosporene (*40*). However, spirilloxanthin was not detected in the cell extract of this mutant grown under the anaerobic condition in a previous study (*32*). In this study (Table S1 of the Supporting Information), spirilloxanthin was not detected in either chromatophores or LH2 at all but was detected in the RC. The accumulation of such a small amount of spirilloxanthin in the RC suggests selective binding.

Mutant, Grown under Semiaerobic Conditions. Car ($n = 9$) with and without the OH group and Car ($n = 10$) and keto-Car ($n = 10 + 1$) with the OH group are selectively bound to LH2, while Car ($n = 10$) and keto-Car ($n = 10 + 1$) without the OH group are mainly bound to the RC. Here again, Car ($n = 13$) and keto-Car ($n = 13 + 1$), both the leak components through the spirilloxanthin pathway, are selectively bound to the RC.

The binding described above can be generally summarized as follows. (i) OH-Cars are selectively bound to LH2 almost exclusively. (ii) Keto-Cars are bound to both LH2 and the RC. (iii) Shorter chain Cars ($n = 9$ or 10 anaerobically and 10 or $10 + 1$ semiaerobically) are preferentially bound to LH2. (iv) The available Cars with the longest chains are selectively bound to the RC.

Figure 6 depicts the selection of the overall conjugation length. Here, all the Cars are characterized simply by the number of conjugated double bonds (n), including both the C═C (m) and C═O (o) bonds. This classification is based on the idea that the singlet and triplet excited-state energies are determined by the number of conjugated double bonds ($n = m + o$). Here, no differentiation is made between the presence and absence of the OH group. It is generally shown that Cars with a shorter conjugated chain ($n = 9$ or 10 anaerobically and $n = 10$ or 11 semiaerobically) are preferentially bound to LH2, whereas those available Cars with the longest conjugated chain ($n = 13$, 13−15, 10, or 11 depending on the strain and the culturing condition) are preferentially bound to the RC. In the case of the wild type, where those pigment−protein complexes can freely choose the conjugation lengths from a variety of them, this selective binding is clearly seen, irrespective of the anaerobic or semiaerobic culturing conditions. In the case of the mutant, the choice of the conjugation lengths is limited, and as a result, the selective binding becomes less clear.

DISCUSSION

Possible Mechanisms of Selective Binding: Structures of the Car Binding Sites in LH2 and the RC

The structures of the Car binding sites in LH2 and the RC from *Rvi. gelatinosus* are unknown; however, the structure of the binding site in LH2 of *Rhodospirillum molischianum* (*41*) and that in the RC of *Rba. sphaeroides* Y (*42*) are useful in contrasting their structures with each other and in examining the mechanisms of selective binding:

LH2 (see Figure 6c of ref 30). The Car binding site is shifted upward in the figure along the axis normal to the membrane plane. The top part is surrounded by hydrophilic amino acid side chains whereas the bottom part by aromatic amino acid side chains and the macrocycles of B850 BChls. The conjugated chain is surrounded by aromatic amino acid side chains to facilitate the dispersive interaction.

Some time ago, unexpected similarities were found between LH2 from *Rsp. molischianum* and LH1 from other purple bacteria (*43*). Most recently, a close resemblance was found between the structure of LH1 from *Rhodospirillum rubrum* as determined by NMR spectroscopy in solution (*44*) and that of LH2 from *Rsp. molischianum* as determined by X-ray crystallography (*41*). Therefore, the binding site shown in Figure 6c of ref *30* may accommodate not only shorter chain Cars but also the longest chain Car, spirilloxanthin. However, LH2 from the present strain, i.e., *Rvi. gelatinosus*, selectively binds Cars for which $m = 9$ and 10 ($n = 9$, 10, and 11). There must be some structural modification for the selective binding of such shorter chain Cars and for the exclusion of the longest chain Cars for which $m = 13$ ($n =$ 13, 14, and 15).

On the other hand, the structure of LH2 from *Rsp. molischianum* nicely explains the selective binding of OH-Cars with a shorter conjugated chain. The OH group on one side can strongly interact with the hydrophilic amino acid side chains on the upper membrane surface, whereas the conjugated chain of Cars can interact with the BChl macrocycles and the aromatic amino acid side chains on the bottom and the lateral surface of the Car binding pocket. The idea concerning the binding of OH-Cars can be supported by the binding of rhodopin glucoside to LH2 from *Rhodopseudomonas acidophila*, the structure of which has been determined by X-ray crystallography [PDB entry 1KZU (*45*); *46*]. The glucoside group is oriented upward to interact with hydrophilic amino acid side chains and possibly with the aqueous layer.

RC (Figure 6a,b of ref 30). The Car binding site is V-shaped to accommodate the central-bent 15-*cis* Car, spheroidene, for example. One of the stretched conjugated chain extends between a pair of helices, and the other fills a pocket on the surface of the M subunit. Both ends extrude from the hydrophobic sides of the peptide subunit toward the hydrocarbon chains of the lipid layer. As a result, there is no limitation in the length of the Car-conjugated chain. The central-bent 15-*cis* Car is surrounded by many aromatic amino acid side chains and is stabilized by dispersive interaction among the conjugated systems and the hydrocarbon chains of lipid. The longest chain Cars may be stabilized most.

The pictures of the Car binding sites given above explain the selective binding of the shorter chain Cars without and with the OH group to LH2, and the selective binding of the longest chain Cars to the RC.

Possible Reasons for the Selective Binding of Cars in LH2 and the RC

As described in the introductory section, it is likely that the light-harvesting function is most important in LH2, whereas the photoprotective function is most important in the RC. We will try to rationalize the natural selection of the conjugation lengths by LH2 and the RC in relation to their physiological functions on the basis of our recent results of investigations (*15*, *47*).

LH2. Figure 7 (the top panel) graphically shows the efficiency of triplet generation and those of the Car-to-BChl singlet-energy transfer through three channels, i.e., $1B_u^+ \rightarrow Q_x$, $1B_u^- \rightarrow Q_x$, and $2A_g^- \rightarrow Q_y$, in LH2 from *Rba. sphaeroides* G1C, *Rba. sphaeroides* 2.4.1, *Rsp. molischianum*, and *Rps. acidophila* 10050, containing neurosporene ($n = 9$), spheroidene ($n = 10$), lycopene and rhodopin (both $n = 11$), and rhodopin glucoside ($n = 11$), respectively (*15*). The figure shows that all the $1B_u^+$, $1B_u^-$, and $2A_g^-$ channels of singlet-energy transfer are active in Car ($n = 9$) and Car ($n = 10$), but the latter two channels are practically inactive in Cars ($n = 11$). The sums of the efficiencies through the three channels of singlet-energy transfer that were determined by the analysis of excited-state dynamics, i.e., 88, 84, 51, and 54%, nicely correspond to the overall efficiencies that had been determined independently by comparison of the Car fluorescence excitation and absorption spectra after normalization at the Q_x absorption of BChl, i.e., 92, 89, 53, and 56% (*15*). Note that there is a sudden decrease in the extent of Car-to-BChl singlet-energy transfer on going from $n = 10$ to $n = 11$.

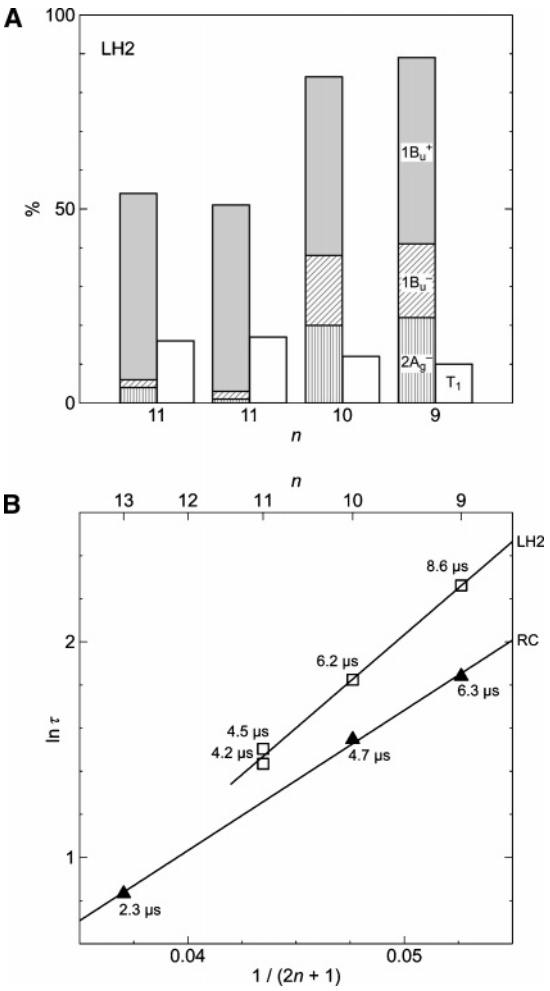

FIGURE 7: (A) Efficiencies of singlet energy transfer from Car to BChl, through the $1B_u^+ \rightarrow Q_x$ (gray), $1B_u^- \rightarrow Q_x$ (oblique lines), and $2A_g^- \rightarrow Q_y$ (vertical lines) channels and the generation of the T_1 state from the $1B_u^-$ state (white bars) in LH2 from *Rba. sphaeroides* G1C, *Rba. sphaeroides* 2.4.1, *Rsp. molischianum*, and *Rps. acidophila* 10050 containing neurosporene ($n = 9$), spheroidene ($n = 10$), lycopene and rhodopin (both $n = 11$), and rhodopin glucoside ($n = 11$), respectively (*15*). (B) Dependence of ln τ (T_1 lifetime) on n, as a linear function of $1/(2n + 1)$, in the same set of LH2 species listed above and the RC from *Rba. sphaeroides* G1C, *Rba. sphaeroides* 2.4.1, and *Rsp. rubrum* S1 containing neurosporene ($n = 9$), spheroidene ($n = 10$), and spirilloxanthin ($n = 13$), respectively (*47*).

Figure 1 (top) shows the energies of the $1B_u^+$, $3A_g^-$, $1B_u^-$, and $2A_g^-$ states of Cars, as functions of $1/(2n + 1)$, which were determined by measurement of resonance Raman excitation profiles of Cars in the crystalline state (*9*). The energies of the Q_x and Q_y states of BChl *a* in LH2, determined by conventional absorption spectroscopy, are also shown for comparison. The efficiency of Car-to-BChl singlet-energy transfer is governed, in general, by the overlap between the fluorescence profile from each singlet excited state of Car (extending downward in the diagram) and the absorption profile from each singlet state of BChl (extending upward), irrespective of the symmetries of the electronic states or the energy-transfer mechanism (through the transition dipole−transition dipole, electron exchange, or more generally Coulombic interaction). Therefore, the relative heights of each pair of singlet states of Car and BChl show that the $1B_u^+$-to-Q_x energy-transfer pathway should be open for all of the Cars ($n = 9-13$). However, the $1B_u^-$-to-Q_x and $2A_g^-$-to-Q_y singlet energy-transfer pathways should be open in Cars ($n = 9$ and 10), but closed in Cars ($n = 11-13$), because, on going from $n = 10$ to $n = 11$, the $1B_u^-$ ($v = 0$) state of Car becomes lower than the Q_x state of BChl and the $2A_g^-$ ($v = 0$) state of Cars becomes too close to the Q_y state of BChl. Thus, the sudden decrease in the singlet energy-transfer efficiency on going from $n = 10$ to $n = 11$ can be nicely explained by the use of the energy diagram. On the other hand, the efficiency of triplet generation increases on going from $n = 9$ to $n = 11$ (Figure 7). Thus, it is rationalized that the shorter chain Cars ($n = 9$ and 10) are selected by LH2 for the light-harvesting function.

This discussion concerning the light-harvesting function and triplet generation via the $1B_u^-$ state is in good agreement with those via the S* state that have been proposed by van Grondelle and co-workers. Gradinaru et al. (*19*) reported, for the first time, the singlet-to-triplet conversion by means of femtosecond time-resolved absorption spectroscopy of spirilloxanthin in the membrane fragments and LH1 from *Rsp. rubrum*. They ascribed the conversion to the intramolecular fission reaction starting from an intermediate singlet state, which was named "the S* state". They inferred that the S* state could be the $1B_u^-$ state reported in spheroidene by Sashima et al. (*7*). Further, Papagiannakis et al. (*48*) examined LH2 from *Rba. sphaeroides* and found that the S* state was actively involved in the Car-to-BChl singlet-energy transfer in competition with the above-mentioned fission reaction to generate the triplet state.

The twisting of the Car-conjugated chain may play an important role in triplet generation and, as a result, affect the Car-to-BChl singlet-energy transfer: Papagiannakis et al. (*49*) showed that spirilloxanthin that was incorporated into the B850 complex from *Rba. sphaeroides* exhibited a triplet yield similar to that of spheroidene (5−10%), although spirilloxanthin in native LH1 exhibited a much higher yield of 25−30%. On the other hand, Hayashi et al. (*50*) showed that the distortion of the Car-conjugated chain can be probed by the use of the 965 cm^{-1} Raman line (the C−H out-of-plane wagging mode) and that the distortion could be correlated with a decrease in the efficiency of Car-to-BChl singlet-energy transfer. By using this method, they showed that the incorporation of spheroidene into the "LH" complex from *Chromatium vinosum* gave rise to the particular Raman line and a reduced energy-transfer efficiency in contrast to the case for the LH complex from *Rba. sphaeroides*. Those results clearly indicate that the structure of the apoprotein plays an important role in determining the singlet energy-transfer efficiency.

This view just focusing on the lengths of the conjugated chain may be too simple, although we believe it is good enough for a first approximation. In this relation, it is worth mentioning that similar and consistent conjugation length dependence was found in LH1 from *Rsp. rubrum* G9 (a Car-less mutant) into which a set of Cars for which $n = 9-13$ had been incorporated (*14*).

RC. No direct singlet-energy transfer takes place from the RC-bound 15-*cis* Cars to special-pair BChls (P) (*51*) because the long axis of the bent 15-*cis* Car and the macrocycle plane of P are almost perpendicular to each other (*42*) and the former is located far from the latter, although very efficient singlet-energy transfer via the accessory BChl (B) has been reported (*52*). However, the most important role of Car in the RC is the dissipation of triplet energy that is transferred from the triplet-state special-pair BChls via B (*53*). Actually, the relevant pigments are nicely arranged to facilitate the triplet-energy transfer in the P → B → Car order (see Figure 5 of ref *54*); those pigments are in close contact as shown by X-ray crystallography (R. J. Cogdell, personal communication). It seems that those pigments including P, B, and Car in the RC are in close contact and nicely arranged to facilitate singlet-energy transfer via the covalent states ($3A_g^-$, $2A_g^-$, and $1B_u^-$) as well as triplet-energy transfer, in each of which the electron exchange mechanism plays a most important role. Figure 1 (bottom) also shows the T_1 energies of BChl *a* and Cars determined by measurement of phosphorescence from a set of LH2 species that were isolated from *Rba. sphaeroides* G1C, *Rba. sphaeroides* 2.4.1, and *Rsp. molischianum* containing neurosporene ($n = 9$), spheroidene ($n = 10$), and lycopene and rhodopin (both $n = 11$), respectively (*55*). The linear relation shows that the T_1 energy is systematically decreased with *n* in comparison to that of BChl; a similar trend is naturally expected for the RC-bound 15-*cis* Cars as well, although the relevant phosphorescence data are still not available. According to this trend and the Englman−Jortner energy-gap law (*56*), the T_1 lifetime (τ) of the RC-bound Car is systematically shortened with *n* as shown in Figure 7 (bottom). Actually, the linear dependence of $\ln \tau$ as a function of $1/(2n + 1)$ shows that the triplet-energy dissipation by 15-*cis*-spirilloxanthin ($n = 13$) is approximately 2.7 times more efficient than that by 15-*cis*-neurosporene ($n = 9$) (*47*), a fact which indicates the advantage of the longest chain Car for triplet-energy dissipation. Thus, it is rationalized that the 15-*cis*-Car having the longest conjugated chain is selected by the RC for the photoprotective function.

CONCLUSION

In this investigation, we have found the following selective binding of Cars to LH2 and the RC in a real living photosynthetic bacterium, *Rvi. gelatinosus*, having both the spheroidene and spirilloxanthin pathways of carotenogenesis. (i) Shorter chain Cars are selectively bound to LH2 whereas longer-chain Cars to the RC. (ii) OH-Cars having a shorter conjugated chain are selectively bound to LH2.

The mechanism of selective binding has been explained in terms of the structures of the Car binding sites. The

binding site in LH2 is normal to the membrane, is shifted toward the membrane surface, and may be limited in the conjugation length of Car accommodated, whereas the binding site in the RC is parallel to the membrane, extruding into the lipid bilayer and having no limitation on Car conjugation length.

The reason for the selection of the conjugation lengths has been rationalized in terms of the excited-state properties and the physiological functions of Cars. The Car-to-BChl singlet-energy transfer is more efficient in shorter chain Cars, whereas the generation and decay of the T_1 state are more efficient in longer chain Cars. In other words, shorter chain Cars are more advantageous for the light-harvesting function, whereas longer chain Cars are more advantageous for the photoprotective function. Those excited-state properties originate from the conjugation length dependence of the singlet and triplet energy levels.

Combining the natural selection of the Car configurations and the natural selection of the Car conjugation length, we now propose the following structural selection of Cars by pigment−protein complexes; all-*trans* shorter chain Cars are selected by LH2 for the light-harvesting function, whereas 15-*cis* longest chain Cars are selected by the RC for the photoprotective function.

ACKNOWLEDGMENT

We thank Dr. Kayoko Saiki and Dr. Yasuo Noda for support in data collection and analyses via mass spectroscopy and 600 MHz ^{1}H NMR spectroscopy, respectively, of the extracted Cars.

SUPPORTING INFORMATION AVAILABLE

Details of carotenoid compositions in chromatophores, LH2, and the RC from *Rvi. gelatinosus* (Table S1). This material is available free of charge via the Internet at http://pubs.acs.org.

REFERENCES

1. Frank, H. A., and Cogdell, R. J. (1993) The Photochemistry and Function of Carotenoids in Photosynthesis, in *Carotenoids in Photosynthesis* (Young, A., and Britton, G., Eds.) 1st ed., pp 252−326, Chapman and Hall, London.
2. Holt, N. E., Zigmantas, D., Valkunas, L., Li, X.-P., Niyogi, K. K., and Fleming, G. R. (2005) Carotenoid cation formation and the regulation of photosynthetic light harvesting, *Science 307*, 433−436.
3. Hanley, J., Deligiannakis, Y., Pascal, A., Faller, P., and Rutherford, A. W. (1999) Carotenoid oxidation in photosystem II, *Biochemistry 38*, 8189−8195.
4. Frank, H. A., and Brudvig, G. W. (2004) Redox functions of carotenoids in photosynthesis, *Biochemistry 43*, 8607−8615.
5. Koyama, Y. (1991) Structures and functions of carotenoids in photosynthetic systems, *J. Photochem. Photobiol. B 9*, 265−280.
6. Koyama, Y., and Fujii, R. (1999) *Cis-Trans* Carotenoids in Photosynthesis: Configurations, Excited-State Properties and Physiological Functions, in *The Photochemistry of Carotenoids* (Frank, H. A., Young, A. J., Britton, G., and Cogdell, R. J., Eds.) pp 161−188, Kluwer Academic Publishers, Dordrecht, The Netherlands.
7. Sashima, T., Nagae, H., Kuki, M., and Koyama, Y. (1999) A new singlet-excited state of all-*trans*-spheroidene as detected by resonance-Raman excitation profiles, *Chem. Phys. Lett. 299*, 187−194.
8. Sashima, T., Koyama, Y., Yamada, T., and Hashimoto, H. (2000) The $1B_u^+$, $1B_u^-$, and $2A_g^-$ energies of crystalline lycopene, β-carotene, and mini-9-β-carotene as determined by resonance-Raman excitation profiles: Dependence of the $1B_u^-$ state energy on the conjugation length, *J. Phys. Chem. B 104*, 5011−5019.
9. Furuichi, K., Sashima, T., and Koyama, Y. (2002) The first detection of the $3A_g^-$ state in carotenoids using resonance-Raman excitation profiles, *Chem. Phys. Lett. 356*, 547−555.
10. Pariser, R. (1956) Theory of the electronic spectra and structure of the polyacenes and of alternant hydrocarbons, *J. Chem. Phys. 24*, 250−268.
11. Callis, P. R., Scott, T. W., and Albrecht, A. C. (1983) Perturbation selection rules for multiphoton electronic spectroscopy of neutral alternant hydrocarbons, *J. Chem. Phys. 78*, 16−22.
12. Tavan, P., and Schulten, K. (1987) Electronic excitations in finite and infinite polyenes, *Phys. Rev. B 36*, 4337−4358.
13. Koyama, Y., Rondonuwu, F. S., Fujii, R., and Watanabe, Y. (2004) Light-harvesting function of carotenoids in photo-synthesis: The roles of the newly found $1^1B_u^-$ state, *Biopolymers 74*, 2−18.
14. Akahane, J., Rondonuwu, F. S., Fiedor, L., Watanabe, Y., and Koyama, Y. (2004) Dependence of singlet-energy transfer on the conjugation length of carotenoids reconstituted into the LH1 complex from *Rhodospirillum rubrum* G9, *Chem. Phys. Lett. 393*, 184−191.
15. Rondonuwu, F. S., Yokoyama, K., Fujii, R., Koyama, Y., Cogdell, R. J., and Watanabe, Y. (2004) The role of the $1^1B_u^-$ state in carotenoid-to-bacteriochlorophyll singlet-energy transfer in the LH2 antenna complexes from *Rhodobacter sphaeroides* G1C, *Rhodobacter sphaeroides* 2.4.1, *Rhodospirillum molischianum* and *Rhodopseudomonas acidophila*, *Chem. Phys. Lett. 390*, 314−322.
16. Wang, P., Nakamura, R., Kanematsu, Y., Koyama, Y., Nagae, H., Nishio, T., Hashimoto, H., and Zhang, J.-P. (2005) Low-lying singlet states of carotenoids having 8−13 conjugated double bonds as determined by electronic absorption spectroscopy, *Chem. Phys. Lett. 410*, 108−114.
17. Tavan, P., and Schulten, K. (1986) The low-lying electronic excitations in long polyenes: A PPP-MRD-Cl study, *J. Chem. Phys. 85*, 6602−6609.
18. Starcke, J. H., Wormit, M., Schirmer, J., and Dreuw, A. (2006) How much double excitation character do the lowest excited states of linear polyenes have? *Chem. Phys. 329*, 39−49.
19. Gradinaru, C. C., Kennis, J. T. M., Papagiannakis, E., van Stokkum, I. H. M., Cogdell, R. J., Fleming, G. R., Niederman, R. A., and van Grondelle, R. (2001) An unusual pathway of excitation energy deactivation in carotenoids: Singlet-to-triplet conversion on an ultrafast timescale in a photosynthetic antenna, *Proc. Natl. Acad. Sci. U.S.A. 98*, 2364−2369.
20. Cerullo, G., Polli, D., Lanzani, G., de Silvestri, S., Hashimoto, H., and Cogdell, R. J. (2002) Photosynthetic light harvesting by carotenoids: Detection of an intermediate excited state, *Science 298*, 2395−2398.
21. Larsen, D. S., Papagiannakis, E., van Stokkum, I. H. M., Vengris, M., Kennis, J. T. M., and van Grondelle, R. (2003) Excited state dynamics of β-carotene explored with dispersed multi-pulse transient absorption, *Chem. Phys. Lett. 381*, 733−742.
22. Kodis, G., Herrero, C., Palacios, R., Mariño-Ochoa, E., Gould, S., de la Garza, L., van Grondelle, R., Gust, D., Moore, T. A., Moore, A. L., and Kennis, J. T. M. (2004) Light harvesting and photoprotective functions of carotenoids in compact artificial photosynthetic antenna designs, *J. Phys. Chem. B 108*, 414−425.
23. Hashimoto, H., and Koyama, Y. (1988) Time-resolved resonance Raman spectroscopy of triplet β-carotene produced from all-*trans*, 7-*cis*, 9-*cis*, 13-*cis*, and 15-*cis* isomers and high-pressure liquid chromatography analyses of photoisomerization via the triplet state, *J. Phys. Chem. 92*, 2101−2108.
24. Hashimoto, H., Koyama, Y., Ichimura, K., and Kobayashi, T. (1989) Time-resolved absorption spectroscopy of the triplet state produced from the all-*trans*, 7-*cis*, 9-*cis*, 13-*cis*, and 15-*cis* isomers of β-carotene, *Chem. Phys. Lett. 162*, 517−522.
25. Kuki, M., Koyama, Y., and Nagae, H. (1991) Triplet-sensitized and thermal isomerization of all-*trans*, 7-*cis*, 9-*cis*, 13-*cis*, and 15-*cis* isomers of β-carotene: Configurational dependence of the quantum yield of isomerization via the T_1 state, *J. Phys. Chem. 95*, 7171−7180.
26. Fujii, R., Furuichi, K., Zhang, J.-P., Nagae, H., Hashimoto, H., and Koyama, Y. (2002) *Cis*-to-*trans* isomerization of spheroidene in the triplet state as detected by time-resolved absorption spectroscopy, *J. Phys. Chem. A 106*, 2410−2421.
27. Ohashi, N., Ko-chi, N., Kuki, M., Shimamura, T., Cogdell, R. J., and Koyama, Y. (1996) The structures of S_0 spheroidene in the light-harvesting (LH2) complex and S_0 and T_1 spheroidene in the

reaction center of *Rhodobacter sphaeroides* 2.4.1 as revealed by Raman spectroscopy, *Biospectroscopy 2*, 59−69.
28. Mukai-Kuroda, Y., Fujii, R., Ko-chi, N., Sashima, T., Koyama, Y., Abe, M., Gebhard, R., van der Hoef, I., and Lugtenburg, J. (2002) Changes in molecular structure upon triplet excitation of all-*trans*-spheroidene in *n*-hexane solution and 15-*cis*-spheroidene bound to the photo-reaction center from *Rhodobacter sphaeroides* as revealed by resonance-Raman spectroscopy and normal-coordinate analysis, *J. Phys. Chem. A 106*, 3566−3579.
29. Kakitani, Y., Fujii, R., Koyama, Y., Nagae, H., Walker, L., Salter, B., and Angerhofer, A. (2006) Triplet-state conformational changes in 15-*cis*-spheroidene bound to the reaction center from *Rhodobacter sphaeroides* 2.4.1 as revealed by time-resolved EPR spectroscopy: Strengthened hypothetical mechanism of triplet-energy dissipation, *Biochemistry 45*, 2053−2062.
30. Qian, P., Saiki, K., Mizoguchi, T., Hara, K., Sashima, T., Fujii, R., and Koyama. Y. (2001) Time-dependent changes in the carotenoid composition and preferential binding of spirilloxanthin to the reaction center and anhydrorhodovibrin to the LH1 antenna complex in *Rhodobium marinum*, *Photochem. Photobiol. 74*, 444−452.
31. Takaichi, S. (1999) Carotenoids and Carotenogenesis in Anoxygenic Photosynthetic Bacteria, in *The Photochemistry of Carotenoids* (Frank, H. A., Young, A. J., Britton, G., and Cogdell, R. J., Eds.) pp 39−69, Kluwer Academic Publishers, Dordrecht, The Netherlands.
32. Harada, J., Nagashima, K. V. P., Takaichi, S., Misawa, N., Matsuura, K., and Shimada, K. (2001) Phytoene desaturase, CrtI, of the purple photosynthetic bacterium, *Rubrivivax gelatinosus*, produces both neurosporene and lycopene, *Plant Cell Physiol. 42*, 1112−1118.
33. Nagashima, K. V. P., Shimada, K., and Matsuura, K. (1996) Shortcut of the photosynthetic electron transfer in a mutant lacking the reaction center-bound cytochrome subunit by gene disruption in a purple bacterium, *Rubrivivax gelatinosus*, *FEBS Lett. 385*, 209−213.
34. Eimhjellen, K. E., and Jensen, S. L. (1964) The biosynthesis of carotenoids in *Rhodopseudomonas gelatinosa*, *Biochim. Biophys. Acta 82*, 21−40.
35. Enzell, C. R., and Back, S. (1995) Mass Spectrometry, in *Carotenoids Volume 1B: Spectroscopy* (Britton, G., Liaaen-Jensen, S., and Pfander, H., Eds.) pp 261−320, Birkhäuser Verlag, Basel, Switzerland.
36. Katayama, N., Hashimoto, H., Koyama, Y., and Shimamura, T. (1990) High-performance liquid chromatography of *cis-trans* isomers of neurosporene: Discrimination of *cis* and *trans* configurations at the end of an open conjugated chain, *J. Chromatogr. 519*, 221−227.
37. Jiang, Y.-S., Kurimoto, Y., Shimamura, T., Ko-chi, N., Ohashi, N., Mukai, Y., and Koyama, Y. (1996) Isolation by high-pressure liquid chromatography, configurational determination by ^{1}H-NMR, and analyses of electronic absorption and Raman spectra of isomeric spheroidene, *Biospectroscopy 2*, 47−58.
38. Lindal, T.-R., and Liaaen-Jensen, S. (1997) Bacterial carotenoids 56. On the spirilloxanthin stereoisomeric set, *Acta Chem. Scand. 51*, 1128−1131.
39. Qian, P., Mizoguchi, T., Fujii, R., and Hara, K. (2002) Conformation analysis of carotenoids in the purple bacterium *Rhodobium marinum* based on NMR spectroscopy and AM1 calculation, *J. Chem. Inf. Comput. Sci. 42*, 1311−1319.
40. Albrecht, M., Takaichi, S., Misawa, N., Schnurr, G., Böger, P., and Sandmann, G. (1997) Synthesis of atypical cyclic and acyclic hydroxyl carotenoids in *Escherichia coli* transformants, *J. Biotechnol. 58*, 177−185.
41. Koepke, J., Hu, X., Muenke, C., Schulten, K., and Michel, H. (1996) The crystal structure of the light-harvesting complex II (B800−850) from *Rhodospirillum molischianum*, *Structure 4*, 581−597.
42. Arnoux, B., Gaucher, J.-F., Ducruix, A., and Reiss-Husson, F. (1995) Structure of the photochemical reaction centre of a spheroidene-containing purple bacterium, *Rhodobacter sphaeroides* Y, at 3 Å resolution, *Acta Crystallogr. D51*, 368−379.
43. Germeroth, L., Lottspeich, F., Robert, B., and Michel, H. (1993) Unexpected similarities of the B800−850 light-harvesting complex from *Rhodospirillum molischianum* to the B870 light-harvesting complexes from other purple photosynthetic bacteria, *Biochemistry 32*, 5615−5621.
44. Wang, Z.-Y., Gokan, K., Kobayashi, M., and Nozawa, T. (2005) Solution structures of the core light-harvesting α and β polypeptides from *Rhodospirillum rubrum*: Implications for the pigment-protein and protein-protein interactions, *J. Mol. Biol. 347*, 465−477.
45. Prince, S. M., Papiz, M. Z., Freer, A. A., McDermott, G., Hawthornthwaite-Lawless, A. M., Cogdell, R. J., and Isaacs, N. W. (1997) Apoprotein structure in the LH2 complex from *Rhodopseudomonas acidophila* strain 10050: Modular assembly and protein pigment interactions, *J. Mol. Biol. 268*, 412−423.
46. Cogdell, R. J., Isaacs, N. W., Freer, A. A., Arrelano, J., Howard, T. D., Papiz, M. Z., Hawthornthwaite-Lawless, A. M., and Prince, S. (1997) The structure and function of the LH2 (B800−850) complex from the purple photosynthetic bacterium *Rhodopseudomonas acidophila* strain 10050, *Prog. Biophys. Mol. Biol. 68*, 1−27.
47. Kakitani, Y., Akahane, J., Ishii, H., Sogabe, H., Nagae, H., and Koyama, Y. (2007) Conjugation-length dependence of the T_1 lifetimes of carotenoids free in solution and incorporated into the LH2, LH1, RC, and RC-LH1 complexes: Possible mechanisms of triplet-energy dissipation, *Biochemistry 46*, 2181−2197.
48. Papagiannakis, E., Kennis, J. T. M., van Stokkum, I. H. M., Cogdell, R. J., and van Grondelle, R (2002) An alternative carotenoid-to-bacteriochlorophyll energy transfer pathway in photosynthetic light harvesting, *Proc. Natl. Acad. Sci. U.S.A. 99*, 6017−6022.
49. Papagiannakis, E., Das, S. K., Gall, A., van Stokkum, I. H. M., Robert, B., van Grondelle, R., Frank, H. A., and Kennis, J. T. M. (2003) Light harvesting by carotenoids incorporated into the B850 light-harvesting complex from *Rhodobacter sphaeroides* R-26.1: Excited-state relaxation, ultrafast triplet formation, and energy transfer to bacteriochlorophyll, *J. Phys. Chem. B 107*, 5642−5649.
50. Hayashi, H., Noguchi, T., and Tasumi, M. (1989) Studies on the interrelationship among the intensity of a Raman marker band of carotenoids, polyene chain structure, and efficiency of the energy transfer from carotenoids to bacteriochlorophyll in photosynthetic bacteria, *Photochem. Photobiol. 49*, 337−343.
51. Lin, S., Katilius, E., Taguchi, A. K. W., and Woodbury, N. W. (2003) Excitation energy transfer from carotenoid to bacteriochlorophyll in the photosynthetic purple bacterial reaction center of *Rhodobacter sphaeroides*, *J. Phys. Chem. B 107*, 14103−14108.
52. Lin, S., Katilius, E., Ilagan, R. P., Gibson, G. N., Frank, H. A., and Woodbury, N. W. (2006) Mechanism of carotenoid singlet excited state energy transfer in modified bacterial reaction centers, *J. Phys. Chem. B 110*, 15556−15563.
53. Frank, H. A., Chynwat, V., Posteraro, A., Hartwich, G., Simonin, I., and Scheer, H. (1996) Triplet state energy transfer between the primary donor and the carotenoid in *Rhodobacter sphaeroides* R-26.1 reaction centers exchanged with modified bacteriochlorophyll pigments and reconstituted with spheroidene, *Photochem. Photobiol. 64*, 823−831.
54. Koyama, Y., Kakitani, Y., Limantara, L., and Fujii, R. (2006) Effects of Axial Coordination, Electronic Excitation and Oxidation on Bond Orders in the Bacteriochlorin Macrocycle, and Generation of Radical Cation on Photo-Excitation of in vitro and in vivo Bacteriochlorophyll *a* Aggregates: Resonance Raman Studies, in *Chlorophylls and Bacteriochlorophylls: Biochemistry, Biophysics, Functions and Applications* (Grimm, B., Porra, R. J., Rüdiger, W., and Scheer, H., Eds.) pp 323−335, Springer, Dordrecht, The Netherlands.
55. Rondonuwu, F. S., Taguchi, T., Fujii, R., Yokoyama, K., Koyama, Y., and Watanabe, Y. (2004) The energies and kinetics of triplet carotenoids in the LH2 antenna complexes as determined by phosphorescence spectroscopy, *Chem. Phys. Lett. 384*, 364−371.
56. Englman, R., and Jortner, J. (1970) The energy gap law for radiationless transitions in large molecules, *Mol. Phys. 18*, 145−164.

BI602485X